

Remote Hyperthermia, Drug Delivery and Thermometry: The Multifunctional Platform Provided by Nanoparticles

Qing Xiang¹ and Paulo Cesar Morais^{2,3*}

¹Wuhan Yangtze Business University, School of Engineering, Wuhan 430065, China

²Universidade de Brasília, Instituto de Física, Brasília DF 70910-900, Brazil

³Huazhong University of Science and Technology, School of Automation, Wuhan 430074, China

Abstract

The huge demand for biocompatible, robust, accurate and noninvasive technology to assess the temperature of a biological targeted site for monitoring the hyperthermia effect brings the topic of remote thermometry to a very high level of interest. There are already promising research directions to fulfil such demand in the short term and a review of the achievements in this issue is certainly worth. This report offers an overview of the research regarding the most promising nanothermometers nowadays, with emphasis on those addressed to remote operation while using optical or magnetic responses of nanosized materials as the thermometric property. More specifically the optical emission intensity, optical emission peak shift and optical emission lifetime will be covered as far as the optical-based nanothermometers are concerned. Additionally, for the magnetic-based nanothermometers the magnetization or the magnetic susceptibility are the thermometric properties covered in this review. Furthermore, the review includes the hyperthermia effect based on nanosized metallic or magnetic particles plus a couple of thermally-responsive polymeric drug delivery systems, aiming to provide an integrated view of the multipurpose platform offered by actuating-sensing nanoparticles. As far as the regulatory system is concerned the availability of noninvasive thermometry incorporating biocompatibility, robustness and accuracy will establish the grounds needed for the approval of the hyperthermia technology for therapeutic purposes, thus allowing the market of this technological option on a global scale.

Keywords: Remote drug delivery; Remote hyperthermia; Remote nanothermometry; Semiconductor nanoparticle; Metallic nanoparticle; Magnetic nanoparticle

Introduction

Sensing temperature, remotely and accurately, using a robust and inexpensive approach is critical to emerging medical and biomedical technologies. Therapeutic hyperthermia, driven either magnetically using nanosized magnetic materials subjected to AC magnetic fields [1,2] or electromagnetically using metallic nanomaterials excited with appropriated light source [3] or radiofrequency field [4,5], is a paramount example of such demand. As a therapeutic modality hyperthermia has focusing on two commonly applied strategies, namely conventional hyperthermia therapy [6] carried out at mild temperature (typically in the range of 42-45°C) and ablation therapy [7] performed at higher temperatures (typically above 50°C). Drug delivery material systems based on thermoresponsive biocompatible templates also represent a key emerging technology, with an enormous demand for remote and accurate temperature measurements [8,9]. The lack of a suitable technological option to assess the temperature of a biological targeted site has delayed the market of both hyperthermia and thermoresponsive drug delivery technologies for clinical use on a large scale, as for instance in cancer therapy [10], gene therapy [11], and thermally-controlled drug delivery protocols [12]. Invasive approaches for monitoring the hyperthermia effect using thermocouples have been employed in phase-I trials, but they are not accurate enough and produce enormous discomfort to the patients [13]. Additionally, invasive approaches monitor the bulk temperature instead, which may differ from the heating-source or drug delivery site remarkably [14]. It is therefore of great interest to develop inexpensive, noninvasive and accurate approaches for measuring temperature, including integration of the biocompatible sensor with a robust protocol to acquire and handle the thermometric property, expected to support breakthroughs in the coming years in basic cell and tissue research as well as in both

hyperthermia and thermoresponsive drug delivery systems for clinical use.

Although nanothermometry is at its infancy considerable progress has been made recently in regard to its use for remote assessing the temperature at the site the nanomaterials are incorporated to. Nanoprobes allowing remote temperature-sensing using optical or magnetic properties are among the most promising directions nowadays. Most of the optical-based nanothermometers use the light-emitting intensity [15-23], light-emitting peak shift [24-26], or lifetime decay of a suitable optical band as the thermometric property [27-30]. As far as the clinical use is concerned the drawbacks of the actual optical-based nanothermometers rely on biocompatibility (usual semiconductor-based core nanoprobes or dye-based shell moieties are toxic), robustness (typical bleaching of organic-based shell moieties) or temperature accuracy (no better than 0.3°C nowadays), or even combination of these factors. Moreover, due to limitations imposed by living tissues on the optical penetration of light (optical therapeutic window in the 700-1100 nm wavelength range), noninvasive clinical use of optical excitation and signal pickup is a huge challenge, not yet solved, except for very special therapeutic applications, as for instance the photodynamic therapy for treatment (heating monitoring) of skin cancer and follow up [31]. Alternatively, the magnetic-based nanothermometry uses magnetization or susceptibility measurements

***Corresponding author:** Paulo Cesar Morais, Universidade de Brasília, Instituto de Física, Brasília DF 70910-900, Brazil, Tel: +55-61-81860788/+86-186-74040962; Fax: +55-61-32723151; E-mail: pcmor@unb.br

Received May 15, 2014; Accepted June 26, 2014; Published June 30, 2014

Citation: Xiang Q, Morais PC (2014) Remote Hyperthermia, Drug Delivery and Thermometry: The Multifunctional Platform Provided by Nanoparticles. J Nanomed Nanotechnol 5: 209. doi: [10.4172/2157-7439.1000209](https://doi.org/10.4172/2157-7439.1000209)

Copyright: © 2014 Xiang Q, et al. This is an open-access article distributed under the terms of the Creative Commons Attribution License, which permits unrestricted use, distribution, and reproduction in any medium, provided the original author and source are credited.

of magnetic nanoprobe for remote assessing site-targeted temperatures [32-35]. Typical magnetic nanoprobe are surface-functionalized cubic ferrites, such as magnetite and maghemite nanoparticles [32-36]. Actually, up to date, for noninvasively clinical use the available data favour magnetic nanothermometry as compared to optical nanothermometry. At the present time key issues such as biocompatibility (magnetite and maghemite nanoparticles are very much biocompatible and already approved by the FDA), robustness (magnetization and susceptibility measurements provide very high repetitiveness, sensitivity, and accuracy) and temperature accuracy (better than 0.5°C nowadays) related to remote magnetic nanothermometry surpass the records of remote optical nanothermometry. Notice, however, that remote magnetic nanothermometry and magnetically-driven hyperthermia can use the same material platform (surface-functionalized and/or encapsulated magnetic nanoparticles), thus allowing integration of heating-sensing functionalities in future hyperthermia- and drug delivery-oriented hybrid nanodevices. Likewise, remote optical nanothermometry and optically-driven hyperthermia can be engineered to use the same nanomaterial (surface-functionalized and/or encapsulated metallic nanoparticles). Nevertheless, a single nanoprobe incorporating biocompatibility, robustness and superior temperature accuracy (improving the actual decimals accuracy to centesimals of degrees centigrade) has not yet been proposed in order to fulfil the required standards for monitoring temperature in basic research as well as for hyperthermia and thermoresponsive drug delivery technologies.

This review aims to provide the latest information regarding the advances on nanothermometry focusing on its application in the nanoparticle-based hyperthermia and thermoresponsive drug delivery technologies. It will be emphasized here how the multifunctional material platform provided by nanosized particles (magnetic or metallic) can be engineered to incorporate noninvasive hyperthermia, drug delivery and thermometry in a single device. Besides the magnetic and metallic nanosized particles addressed in the present review the literature reports alternative nanomaterials currently used as heating devices, such as carbon nanotubes and organic-based nanoparticles [37]. The review is organized as follows: The second and the third sections will present the nanoparticle-based hyperthermia and the thermoresponsive drug delivery backgrounds respectively, emphasizing the need of a remote, accurate, robust and inexpensive approach for temperature measurements. The third section will be restricted to a couple of polymer-based thermoresponsive systems as paramount examples of a very flexible hosting template for both nanoparticles and drugs. The fourth section will report on the state of the art in nanothermometry based on optical and magnetic temperature nanoprobe and their correlation with hyperthermia and thermoresponsive drug delivery technologies. The final section will summarize this review while adding some insights that may be useful for a broader audience.

Nanoparticle-based Hyperthermia

Hyperthermia is indeed a very old approach in clinic. In the ancient Greek medicine Hippocrates (460-370 BC), known as the Father of Modern Medicine, firstly wrote: "*Quae medicamenta non sanat; ferrum sanat. Quae ferrum non sanat; ignis sanat. Quae vero ignis non sanat; insanabilia reportari oportet*". More recently, invasive as well as noninvasive approaches have been developed and addressed to promote hyperthermia, with emphasis as a therapeutic modality for oncology. Among the invasive approaches there is the radio frequency ablation (RFA) technique which is based on the implant of a needle electrode, usually guided by ultrasound imaging into the tumor region, that can

be used for heating the targeted site to temperatures in the range of 60 to 100°C by applying an external radiofrequency field [38,39]. Recent development in RFA includes the incorporation of absorptive mediators into the needle electrode, such as gold nanoparticles, which increases the specificity of the therapy while protecting the normal tissues, as the energy requirement is lowered [40]. Noninvasive approaches, however, represent nowadays the forefront of the hyperthermia research for clinical and drug delivery applications, aiming to be approved by the regulatory agencies in order to reach the global market in the coming years. Nanotechnology provides mainly two different approaches for noninvasive (remote) hyperthermia, both using biocompatible nanosized materials. The first approach is based on metallic materials, mostly gold nanoparticles, which can be accumulated on the targeted site and remotely-activated to act as heat spots by applying near infrared (NIR) light or radiofrequency (RF) fields. Alternatively, the second approach uses magnetic materials, usually cubic ferrite nanosized particles, which can be delivered at the targeted site for further activation by applying external AC magnetic fields in order to produce local heat. By using either the optically- or the magnetically-activating mechanisms the on-site produced heat is transferred into the surrounding volume and can be used for instance to promote cell and tissue damage or can be used to modulate drug delivery from a thermoresponsive hosting template. In all cases, however, the thermal response depends on how much the on-site temperature is upshifted, which critically determines the therapeutic outcome or the drug delivery doses. For instance, in the hyperthermia therapy cancer cells trigger apoptosis typically around 44°C whereas cancer cell necrosis starts around 50°C [41-43]. Either for apoptosis or necrosis the triggering temperature value may varies from tissue to tissue, from one type of cancer cell to another, as well as from one patient to another. Therefore, the nanoparticle hyperthermia (NHT) or the thermoresponsive drug delivery (TDD) technologies critically depend on the development of an approach for temperature measurement, expected to be noninvasive, robust, accurate, and inexpensive. At this point it is interesting to emphasize that both magnetic and metallic nanoparticles can be used not only to produce heat but also to provide the thermometric property, optical or magnetic, to build a remote and suitable nanothermometer. Nanosized cubic ferrites can be used as remotely-driven heaters [41] while providing remote temperature sensing using temperature-dependent magnetic properties [32-35]. Likewise, the metallic nanoparticle-based platform can be used for remote heating [44-46] as well as for remote temperature sensing [47,48]. In this regard the gold nanoparticle-based thermometer already reported involves the surface functionalization of the nanoparticle with molecular species presenting temperature sensitive refractive index, thus modulating the surface gold plasmon resonance peak position. Nevertheless, comparatively, it is clear the superiority of the magnetic-based hyperthermia and nanothermometry for clinical use, as the magnetic excitation as well as the pickup signal from deep tissues do not present the drawbacks presented by the optically-based excitation and detection.

Different synthesis routes have been used to produce noble metal nanoparticles, particularly silver and gold, in the diameter range of 2-100 nm. The typical synthesis for very small and spherical nanoparticles (in the lower end of the 2-100 nm range) involves the reduction of the metal ion with a strong reducing agent in the presence of thiol molecules [49]. In this synthesis route the as-produced metal nanoparticles are immediately surface-dressed with molecules added into the reaction medium. Using this approach thiol-decorated gold nanoparticle (GNP) was surface-functionalized with paclitaxel [50]. A different strategy for the synthesis of silver, gold and bimetallic

silver-gold nanosized particles, incorporating the capability to produce different shapes, is the plasmon-mediated approach [51]. The plasmon-mediated synthetic route has been successfully used to produce nanoparticles with a variety of shapes and sizes, modulated by the composition of the starting chemical reaction medium (the growth solution) and illuminating light-source characteristics. Typically, in this chemical synthesis route, the growth solution to be light-irradiated already contains nanosized metal particles (seed particles) and surface stabilizing agents [51].

Nanosized surface-decorated noble metal particles, as for instance GNPs have been engineered to promote hyperthermia either using NIR light source or RF applied fields, mostly for applications in cancer therapy [44-46]. Whereas the GNP's surface moiety is meant to improve the biocompatibility and/or to provide targeting specificity the Au-core is the heat-generating component while excited by the NIR irradiation or RF field [52-54]. A variety of cancer targeting small molecules and antibodies already approved by the FDA can be used to decorate the GNP, providing them with the specificity to be delivered to malignant cells and tissues. Among small molecules one emphasizes tamoxifen and gefitinib that can be used to bind respectively to the estrogen and epithelial growth factor receptors and therefore suitable to surface-dress the GNP in order to target breast cancer [55] and lung cancer [56] cells and tissues, respectively. Likewise, the FDA approved antibody trastuzumab binds to HER2 receptors and can be used as moieties at the GNP's surface to target breast cancer cells and tissues [57]. A very promising cancer targeting surface moiety is represented by cell-penetrating peptides, as for instance the 86 amino acid HIV-1 tat peptide, successfully attached onto the GNP surface and revealed quick cell internalization and localization in the nucleus [58]. Additionally, selective delivery of GNP to tumor cells has been achieved by covalent coupling surface-functionalized GNP to retargeted adenoviral vectors, thus opening up the opportunity for hyperthermia and gene delivery combined into a multipurpose therapeutic platform [52].

The mechanism behind the hyperthermia effect while NIR light interacts with GNP is the oscillation of the free electron plasma in the gold metal driven by the applied electromagnetic field. Particularly interesting is the enhancement of the heat dissipation as the illuminating electromagnetic wavelength matches the surface plasmon resonance (SPR) frequency [59]. Typically, GNP absorbs light in the region from 500 to 800 nm, which covers an important part of the optical therapeutic window (700-1100 nm), meaning the wavelength the light penetrates deeper into biological media (organs, tissues, and cells) [60]. As the light shines onto the GNP it can be absorbed and further dissipated as heat; or it can be absorbed and re-emitted at the same frequency (Rayleigh scattering); or it can be absorbed and re-emitted with upshifted (Raman anti-Stokes scattering) or downshifted frequency (Raman Stokes scattering) [61]. The typical optical absorption spectra of GNPs depend for instance upon the material system's design (core or core-shell nanostructure), size and shape, thus providing a broad flexibility for engineering GNPs in order to meet specific applications. The tunability of the SPR frequency can go from the visible (528 nm), as for instance in the case of 40 nm average diameter Au-core nanoparticles [62], up to the near infrared (800 nm), as for the case of Si-Au core-shell nanoparticles with Si-core diameter around 120 nm and Au-shell thickness around 15 nm [63]. Additionally, as one reduces the size of the Au-core the SPR frequency shifts upward. Alternatively, as one changes from the Au-core (say 150 nm average diameter) nanostructure to the SiO₂-Au core-shell (say 120 nm SiO₂-core diameter plus 15 nm Au-shell thickness) the SPR frequency shifts downward [64]. Indeed, interaction

between the surface-moieties and the surface plasmon modes also shifts the SPR frequency [65]. The task of estimating the temperature upshift due to an ensemble of GNPs distributed throughout a targeted volume involves the calculation of the effective heat generated while the system is exposed to a given light source. The effective heat generation, usually expressed as the specific absorption rate (SAR, units of W/m³), is given by [66]:

$$SAR = N C_{abs} F = \mu_a F, \quad (1)$$

where N (units of m⁻³) is the number of GNPs per cubic meter, C_{abs} (units of m²) is the absorption cross-section area and F (units of W/m²) is the light source fluence. Whereas the estimation of the absorption cross-section area needs to take into account the actual GNP absorption spectrum calculation of the light source fluence involves the solution of the radiative transport equation [67]. Actually, the radiative transport equation (RTE) is an integro-differential equation which needs to be solved for the radiance. The fluence (F) is then obtained from the spatial integration of the radiance (L) given the characteristics of the light source, absorption coefficient, scattering coefficient, and the scattering phase function. Exact solutions of the RTE can be accomplished in very simple cases only whereas several approximations have been proposed to allow comparison between numerical RTE's solutions and experimental data recorded from laser illumination of GNPs [68,69].

Cubic ferrite-based nanosized particles, such as magnetite and maghemite, can be produced using different chemical synthesis routes. Chemical coprecipitation is a straightforward approach (and the easiest route for scaling up) to obtain cubic ferrite-based nanoparticles. Magnetite nanoparticle has been successfully precipitated in alkaline medium from aqueous solutions containing Fe²⁺ and Fe³⁺ salts (Fe²⁺/Fe³⁺ = 0.5) [70]. The weakness of this synthetic route, however, is the difficulty in controlling the average particle size while producing narrow particle size distributions. The size, shape and composition of the cubic ferrite-based nanoparticles depend on the type of salts used (organic or inorganic), M²⁺/Fe³⁺ ratio (where M=Fe, Co, Ni, Mn, Zn,...), reaction temperature, reaction stirring speed, pH value, and ionic strength of the media [71-73]. An alternative approach for the synthesis of cubic ferrite-based nanosized particles is the thermal decomposition of organometallic compounds in the presence of stabilizing surfactants at higher temperatures using organic solvents as the reaction media [74,75]. Differently from the coprecipitation route thermal decomposition of organometallic precursors provides high quality samples with good control of the sample's crystallinity, precise average size control, and narrow particle size distribution. The drawbacks of this chemical route, however, reside on the amount of material produce in a single batch and the complete removal of non-biocompatible surfactants or non-polar solvents, the former negatively impacts the scaling up of the process whereas the latter limits the use of the nanoparticles for medical and biomedical applications [76].

Surface-functionalization of cubic ferrite-based nanoparticles with small organic molecules, aiming either the targeting of specific cells and tissues or simply a pre-coating for further decoration, has been successfully accomplished during the last decade. Modulation of the citrate surface-grafting onto cobalt ferrite nanoparticles was successfully achieved by varying the pH of the solution the bare particles were treated with [77]. Meso-2,3-dimercaptosuccinic acid (DMSA) has been used for surface-functionalization of bare maghemite nanoparticles at increasing surface-grafting values, revealing a rich scenario of inter-particle and intra-particle linking via disulfide bridges resulting from the oxidation of neighboring thiol groups [78]. The biodistribution and

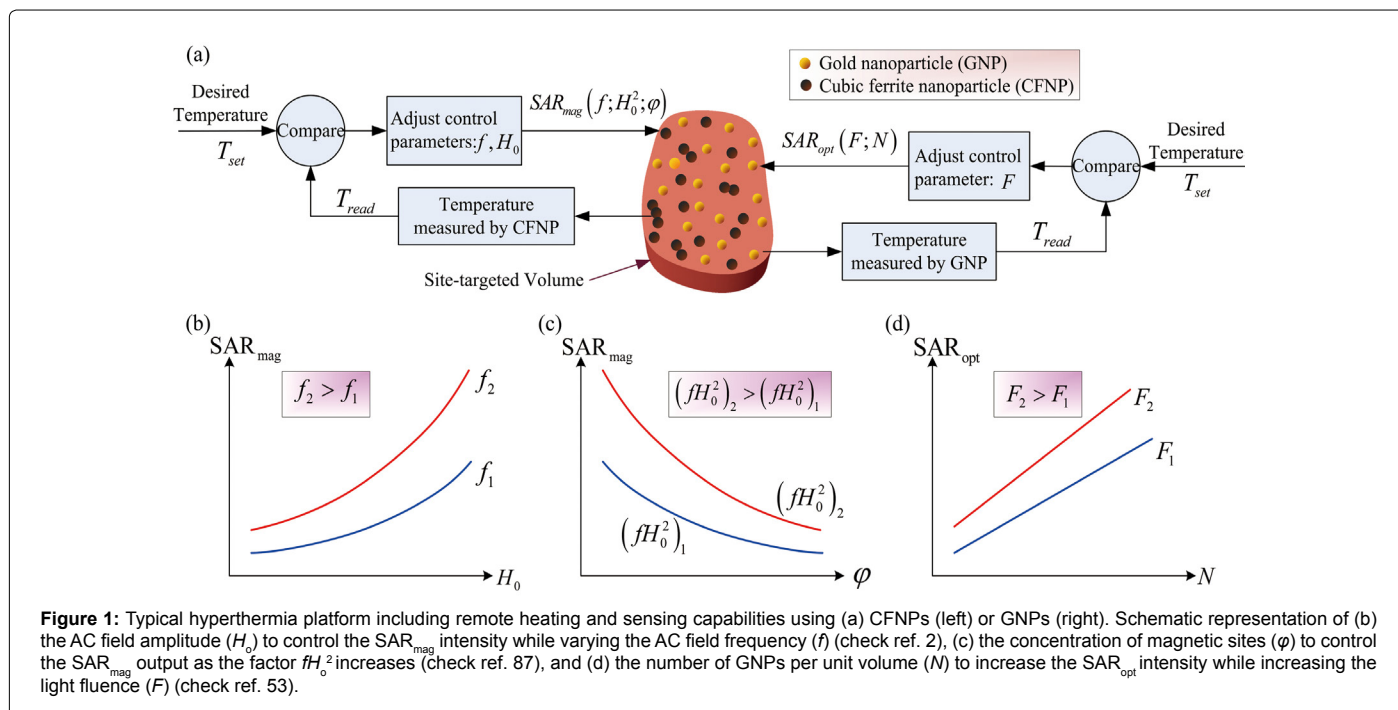
biocompatibility of DMSA-coated maghemite nanoparticles have been recently tested in non-human primates [79]. DMSA-coated magnetic nanoparticles were conjugated to amine-functionalized poly-ethylene glycol (PEG) and revealed reduced internalization in cancer cell lines and extended circulation time in *in vivo* assays [80]. Amphotericin B has been immobilized onto magnetite nanoparticles previously surface-coated with a double layer of oleic acid [81] and further tested for drug delivering against fungal infection in mince lungs [82]. Anti-human cTnI antibody was immobilized onto DMSA-coated magnetic nanoparticles for detection of myocardial injury [83]. Likewise, DMSA-coated maghemite nanoparticle was used to immobilize anticarcinoembryonic antigen (anti-CEA) to successfully target cell lines expressing the CEA, characteristic of colorectal cancer cells [84]. Indeed, regarding cubic ferrite nanosized particle (CFNP) two key aspects should be emphasized at this point: firstly, while presenting ferrimagnetic-superparamagnetic ordering CFNPs strongly interact with applied DC and AC magnetic fields; secondly, due to the reactive amphoteric surface metal sites CFNPs provide a very flexible material platform for immobilization of negatively- as well as positively-charged functional groups found in a huge variety of therapeutic molecules. These two characteristics are key elements for hyperthermia and drug delivering combined into a multipurpose therapeutic material platform.

The mechanism behind the hyperthermia effect promoted by CFNPs is the dynamic response of the particle's magnetization while driven by external AC magnetic fields. The literature reports on the observation of the hyperthermia effect while using AC magnetic fields with amplitudes and frequencies below 0.1 T and 1 kHz, respectively [85,86]. Particularly interesting is the modulation of the heat dissipation as isolated nanoparticles bind together to build in chain-like structures [87]. The physical picture of the magnetohyperthermia effect can be assessed by looking at the interaction between the nanoparticle's magnetic moment and the applied AC magnetic field. While following the rotating magnetic field (AC field) the nanoparticle's magnetic moment may lag behind it at a given phase-shift due to mainly two

aspects; the anisotropy energy barrier of the particle compared to the thermal energy and the particle-particle interaction. This phase-shift gives rise to an in-phase response (real component) plus an out-of-phase response (imaginary component) of the magnetic moment with respect to the applied magnetic field (magnetic susceptibility). The out-of-phase response (imaginary susceptibility) is the one connected to the heat dissipation in the magnetohyperthermia effect. The task of estimating the temperature upshift due to an ensemble of CFNPs distributed throughout a targeted volume involves the calculation of the heat generated as the system is exposed to a given AC magnetic field. This is accomplished by calculating the increase of the internal energy in an adiabatic given cycle. The thermal power (P , units of W) dissipation per unit volume is described by [1]:

$$P = \pi \mu_0 \chi'' f H_0^2, \quad (2)$$

where μ_0 ($4\pi \times 10^{-7}$ T×m/A) is the magnetic permeability of the vacuum, χ'' is the out-of-phase (imaginary) susceptibility, and f (Hz) is the frequency of the applied magnetic field with amplitude H_0 (A/m). Analysis of Eq. (2) shows that the power dissipation can be modulated either by changing the equipment's set up (frequency and field amplitude) or by engineering the sample's characteristics via the response of the imaginary component of the susceptibility (χ''). Instrumental design limits the operation of the equipment at combined higher frequencies and higher field amplitudes. Alternatively, the material's engineering provides a broader flexibility for tuning the thermal flow outputs by adjusting the material's magnetic response via the out-of-phase component of the susceptibility (χ''). Typically, the temperature (T) dependence of the imaginary component of the susceptibility (χ'') presents a bell-shaped curve, shifting its maximum toward higher temperatures as the AC frequency increases [88]. Furthermore, the maximum of the χ'' versus T curve also shifts to higher temperature values as the particle-particle interaction increases [89]. Then, the imaginary component of the susceptibility (χ'') depends on the particular CFNP under consideration and on the particle's shape, average size, and size dispersion [1]. Therefore, the specific absorption rate (SAR, units of W/m³) for magnetohyperthermia is given by:



$$SAR = (C\rho/\varphi)P, \quad (3)$$

where C is the specific heat of the medium, ρ is the mass density of the medium, φ is the concentration of magnetic sites in the medium per unit mL, and P is given by Eq. (2). Notice, however that the concentration of magnetic sites per unit volume (φ) scales linearly with the particle volume fraction (ϕ).

Figure 1 summarizes the parameters and the trends reported for the specific absorption rate (SAR) using metallic (GNP) as well as magnetic (CFNP) nanosized particles. Figure 1a emphasizes the remote strategy for the heating-sensing capability provided by GNPs and CFNPs while targeting a given volume (V). Remote sensing of the local temperature (T_{read}) provides the reference to fine tuning the instrument's output (thermal dissipation) in order to set the required operation profile (T_{set}). Figure 1b shows the trend of the magnetic specific absorption rate (SAR_{mag}) as a function of the amplitude of the AC applied field (H_0) for increasing AC frequencies ($f_2 > f_1$) [2]. Figure 1c shows the trend of the SAR_{mag} while increasing the concentration of the magnetic sites per unit volume (φ). Worth mentioning the key combination of frequency (f) and magnetic field amplitude (H_0) into the parameter fH_0^2 as the increase of φ may lead to the onset of magnetic chain-like structures, thus affecting the thermal dissipation remarkably [87]. Figure 1d shows the trend of the optical specific absorption rate (SAR_{opt}) as a function of the number of metallic nanoparticles per unit volume (N) at increasing values of the light source fluence (F) [53].

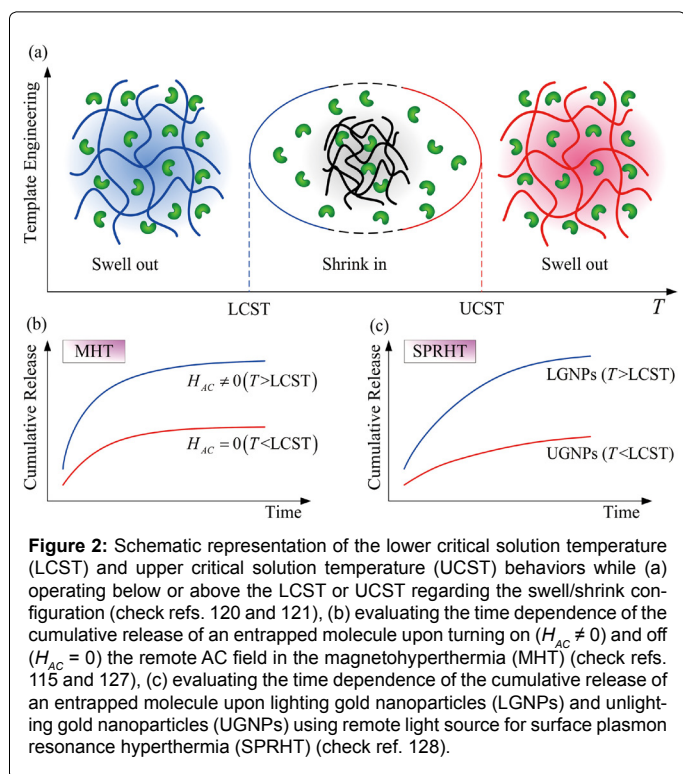
Thermoresponsive Drug Delivery Systems

Encapsulation of GNPs or CFNPs into dielectric hosting templates has been widely reported for over a decade. Aiming different applications *one pot* or *in situ* [90-93] as well as *ex situ* [94-98] approaches for nanoencapsulation can be realized, meaning the strategy of nanoparticle's synthesis simultaneously with the hosting template (*one pot*) or within the reactive hosting template (*in situ*)

for the former and encapsulation of pre-synthesized nanoparticles for the latter. In addition to encapsulation of nanosized particles into biocompatible hosting templates therapeutic molecules can be included for further delivery as well, either within the template [99-108] or decorating the outer surface of the template or, alternatively, decorating the encapsulated nanoparticles [109-114]. Indeed, vectorization of these material systems to target specific cells and tissues can be realized extrinsically using gradients of magnetic fields [10] or intrinsically by dressing the materials' surface with cell receptor-responsive moieties [84,115].

Biocompatible and thermoresponsive templates with reversible properties add extra functionality for the engineering of drug delivery systems (DDS). In particular, polymeric templates should be emphasized, as for instance hydrogels and polymersomes, once they offer a wide variety of opportunities for drug delivering at physiological conditions [116-118]. Basically, a great number of the available thermoresponsive polymeric systems can be grouped into two main categories: the first presents a lower critical solution temperature (LCST) whereas the second reveals an upper critical solution temperature (UCST). The polymeric template shrinks in (swells out) above (below) and below (above) the typical LCST and UCST temperatures, respectively. The physical picture behind this peculiar thermal response is provided by the Gibbs equation of thermodynamics, $\Delta G = \Delta H - T\Delta S$, where ΔG is the Gibbs free energy change, ΔH is the enthalpy change, ΔS is the change in entropy, and T is the absolute temperature of the polymeric template. Favourable transition (shrunk \leftrightarrow swelled) takes place spontaneously as long as the Gibbs free energy faces reduction ($\Delta G < 0$). Such a spontaneous transition is dictated by balancing enthalpy changes (ΔH) against changes in entropy (ΔS) at a typical absolute temperature (T). The enthalpic-dominated ($\Delta H < 0$) swelling of hydrophilic LCST polymers in water is mainly dominated by the hydrogen bonds formed between the polar groups along polymer chains and water molecules. Differently, the entropic-dominated ($\Delta S > 0$) swelling of hydrophilic UCST polymers in water is driven by the mixing between the solvent and the polymer chains. Therefore, as far as the shrunk-swelled transition is concerned LCST (UCST) polymers are enthalpically (entropically) driven [119]. Obviously, the delivery of a therapeutic molecule out from a thermoresponsive polymeric template takes place while the material system evolves from the swelled towards the shrunk phase. The enormous flexibility of delivery modulation provided by thermoresponsive polymers relies on the feasibility of shifting up and down the LCST and UCST values within the physiological and therapeutic ranges, which can be accomplished by engineering the polymeric composition [120].

Hydrogels and polymersomes are among the available thermoresponsive and biocompatible polymers that have been used to incorporate therapeutic molecules plus GNPs or CFNPs, the latter aiming to promote remote and controlled hyperthermia in order to modulate the delivery of the former. Hydrogels are water-based polymer networks, classified either as covalently linked polymers networks in which the polymer chains are linked together via covalent bonds at the crosslink points or as physical gels characterized by the physical entanglement of polymer chains with no covalent bonds between them [121]. On the other hand, polymersomes are vesicular-shaped micelles based on self-assembled amphiphilic block copolymers comprising an insoluble (hydrophobic) and a soluble (hydrophilic) polymer block. Actually, the end amphiphilic-based polymeric micelle morphology is governed by the following parameters: the hydrophobic content, the interfacial hydrophobic-hydrophilic area, and the hydrophobic chain length [122,123].



Meenach et al. [124] have reported the successful fabrication of PEGMA (poly-ethylene glycol methacrylate) hydrogels containing iron oxide nanoparticles for application in drug delivery using magnetohyperthermia. The magnetic PEGMA-based hydrogel is a typical LCST thermoresponsive system, thus presenting deswelling upon heating via AC magnetic field excitation. Likewise, Papaphilipou et al. [125] synthesized PEGMA-based hydrogels incorporating nanosized magnetite particles for drug delivery upon heating using the magnetohyperthermia effect. Polymersome based on poly-trimethylene carbonate-b-poly-L-glutamic acid (PTMC-b-PGA) block copolymer was used to encapsulate nanosized maghemite particles and doxorubicin aiming the delivery of the chemotherapeutic drug upon excitation with AC applied magnetic fields [10]. The diagram in Figure 2a summarizes the delivery of a therapeutic molecule out from a thermoresponsive hosting template while heating up (cooling down) a LCST (UCST) polymer across the typical transition temperature. Worth mentioning that the typical transition temperature associated to the polymeric template (LCST and UCST) can be modulated by engineering the material. Figure 2b shows the trend of the therapeutic molecule cumulative release out from a LCST polymeric template upon remote magnetohyperthermia (MHT) activation while applying ($H_{AC} \neq 0$) an AC magnetic field or switching off ($H_{AC} = 0$) the magnetic field [10,126]. The trends revealed in Figure 2c represent the typical cumulative release of a therapeutic molecule out from a LCST polymeric template using the hyperthermia effect provided by remote excitation of encapsulated GNPs [127]. The cumulative release using the surface plasmon resonance hyperthermia (SPRHT) is much higher under illumination (LGNPs) as the DDS temperature can be driven above the typical LCST ($T > LCST$). Under no illumination (UGNPs), however, the temperature template can be kept below the typical LCST ($T < LCST$) with reduced cumulative release.

Worth mentioning the influence of the finite thermal conductivity of the interface between the heating center and the surrounding medium while evaluating the efficiency of the hyperthermia effect. Citrate-coated-Pt and alkanethiol-terminated-Au nanoparticles (around 10 nm in diameter), respectively suspended in water and toluene, were investigated in regard to the heat transfer efficiency to the surrounding medium (thermal conductivity) while activated by a sub-picosecond laser line from a Ti:Sapphire laser (770 nm wavelength) [128]. The experimental values of the thermal conductance of the suspended Pt-based and Au-based nanoparticles were found to be around 130 and 5 MW/m²K, respectively. Calculation based on the diffuse-mismatch model [129] provided values of 62 and 12 MW/m²K for the Pt/water and Au/toluene interfaces, respectively. Baffou et al. [130] successfully used the discrete dipole approximation and the Green dyadic tensor method to calculate the steady-state temperature distribution in the vicinity of an optically-excited plasmonic nanosized system. Alper and Hamad-Schifferli [131] evaluated the thermal conductivity of gold nanorods surface-coated with hydrophilic and hydrophobic moieties. The authors found that the ability of the surface-coating layer to exclude or include water at the surface of the nanosized structure can be used to modulate the thermal conductance leading to higher or lower values, respectively [131].

Remote Nanoparticle-based Nanothermometers

Emergent biomedical technologies demand the development of new approaches for remote, accurate, robust and inexpensive temperature measurements around the physiological and therapeutic ranges. In this regard nanotechnology has a huge potential to provide solutions to the emergent biomedical fields. A very much promising

direction nowadays is represented by remotely recording a suitable thermometric property following noninvasive excitation of engineered nanosized material structures. More specifically, two approaches are currently under development. Whereas the first approach is based on optically-responsive thermometric properties the second one focuses on magnetically-responsive materials. In both cases the key aspect is the remoteness while exciting and picking up the signal for temperature measurement.

Regarding the optical-based nanothermometer the usual thermometric properties rely on one among the following three options: (1) the temperature dependence of an optical band-intensity or relative-intensity; (2) the temperature dependence of the peak-position of a particular optical emission; or (3) the temperature dependence of a particular optical emission lifetime. The material platform typically includes metallic or semiconductor nanoparticles or optically-active moieties supported onto nanosized structures. The physics behind the selected thermometric property varies substantially and the well-established behaviour will be outlined below.

The temperature (T) dependence of the integrated emission intensity (I) is mainly dominated by the behaviour of the oscillator strength (S) associated to that particular optical transition, as the former (I) scales with the latter (S). The approach behind the calculation of the oscillator strength depends upon the material under consideration (conductor, semiconductor, or insulating). In the temperature range of biomedical applications semiconductor-based nanothermometers show a monotonic and steep decrease of the integrated emission intensity (I) as the temperature (T) increases. This behaviour is mainly due to the presence of the temperature dependence of non-radiative recombination mechanisms and follows the Arrhenius-like law:

$$I = I_0 / \{1 + \sum A_n \exp[-(E_n/kT)]\}, \quad (4)$$

where the sum in Eq (4) runs over a number of contributions (different thermal-activated mechanisms), I_0 is the integrated emission intensity at low temperatures, A_n are dimensionless weighting coefficients, E_n are thermal activation energies, and k is the Boltzmann constant (1.38×10^{-9} J/K). Actually, Eq (4) describes quite well the behaviour of nanothermometers based on II-VI semiconductor structures and polymeric-based semiconductors, which were reported to achieve temperature measurement accuracy of 0.02 [15] and 1°C [19], respectively. Alternatively, optically-active moieties supported onto nanosized structures show a monotonic increase of the integrated emission intensity as the temperature increases. This behaviour, however, is more likely associated to a molecular symmetry-forbidden optical transition that can couple to an allowed transition via a non-totally symmetrical vibrational mode. The population of the vibrational mode increases as the temperature increases, resulting in the increase of the oscillator strength [132]. Hybrid silica nanoparticles decorated with fluorescent precursor were used as a nanothermometer to probe temperature in the range of 20 to 37°C, with accuracy of about 0.1°C [17]. Finally, the iron oxide nanoparticle surface-decorated with a luminescent and thermo-sensitive organic molecule can be used as a nanothermometer, providing spatial resolution in the subnanometer range [23].

The physics behind the temperature (T) dependence of the optical emission wavelength (λ) of metallic nanoparticles is well-described by the Mie's theory [133] whereas the band-gap shrinking of semiconductor nanoparticles accounts for the red-shift of the emission spectra upon heating. Metallic nanoparticles may display either monotonic red-shift or blue-shift of the optical emission

wavelength as the temperature increases, depending upon the dielectric constant of the nanoparticle hosting medium. GNPs supported onto glass substrate interfacing with air (displaying red-shift of the optical emission wavelength) or with water (showing blue-shift of the optical emission wavelength) were successfully used to probe temperature in the range of 27 to 427°C, with accuracy of 2°C [26]. Likewise, a hybrid system comprising gold-magnetite nanoparticles was used to remotely measure (GNP) and increase (CFNP) the temperature in the range of 15 to 40°C, with accuracy of 0.5°C [25]. Alternatively, it has been reported that nanosized semiconductor structures also display a monotonic red-shift of the optical emission energy (E) as the temperature (T) increases [134]. This behaviour is usually described by the empirical Varshni equation [135]:

$$E = E_0 - \alpha T^2 / (\beta + T), \quad (5)$$

where E_0 is the semiconductor band gap at 0 K and α and β are the fitting (Varshni) parameters. Note, however, that Eq. (5) has been successfully used to fit the experimental data for both indirect and direct gap bulk semiconductor materials. Nevertheless, different expressions have been proposed to fit the temperature dependence of the optical emission of bulk semiconductors [136]. Actually, the temperature (T) dependence of the optical emission energy (E) for nanosized semiconductor structures is even more complex, being strongly size dependent [137]. Whereas the 3.9 nm average diameter PbSe quantum dot displays a monotonic red-shift of the optical emission energy (E) as the temperature (T) increases in the range of 300 to 400 K the 6.9 nm average diameter PbSe quantum dot displays a monotonic blue-shift in the same temperature range [138]. The change of signal observed in the rate of the band gap energy with respect to the temperature for

semiconductor quantum dot structures has been mainly assigned to quantum size effects [139,140].

Finally, the lifetime associated to a particular optical transition has been successfully used in nanothermometry. Regardless the specific optical transition under consideration the Arrhenius-like equation describes fairly well the relationship between the lifetime (τ) and the temperature (T) [141]:

$$\tau = \tau_0 / \{1 + (\tau_0 / \tau_b) \exp[-(E_b / kT)]\}, \quad (6)$$

where τ_0 is the decay time at low temperatures, τ_b is the typical decay time, and E_b is the activation energy. The lifetime behaviour of a rhodamine-like moiety immobilized within silica-hybrid nanostructure [28] or at the surface of nanosized gold structures [30] have been used as a nanothermometer in the temperature range of 25 to 55°C (with accuracy of 0.3°C) and 20 to 60°C, respectively. Terbium (III) encapsulated as a complex within a polymeric nanoparticle has been used as a nanothermometer in the temperature range of 15 to 65°C [27]. Actually, the usual thermometric properties assessed from rare-earth doped materials, such as the temperature dependence of the emission intensity [24,25] and lifetime [32], particularly in the case of thermally-coupled optical transitions, are not easily described.

The thermometric property of magnetic-based nanothermometers proposed up to date is either based on magnetization [33-35] or susceptibility [32] measurements. Similarly to the optical approaches magnetic-based nanothermometry relies on remote excitation as well as on remote detection of the thermometric magnetic property. The physics behind the magnetic nanothermometry is the magnetic response of non-interacting nanosized magnetic particles above the blocking temperature (T_b), namely in the superparamagnetic regime. The temperature (T) and the field (H) dependence of the magnetization (M) of a superparamagnetic sample is governed by the first-order Langevin function [1,2]:

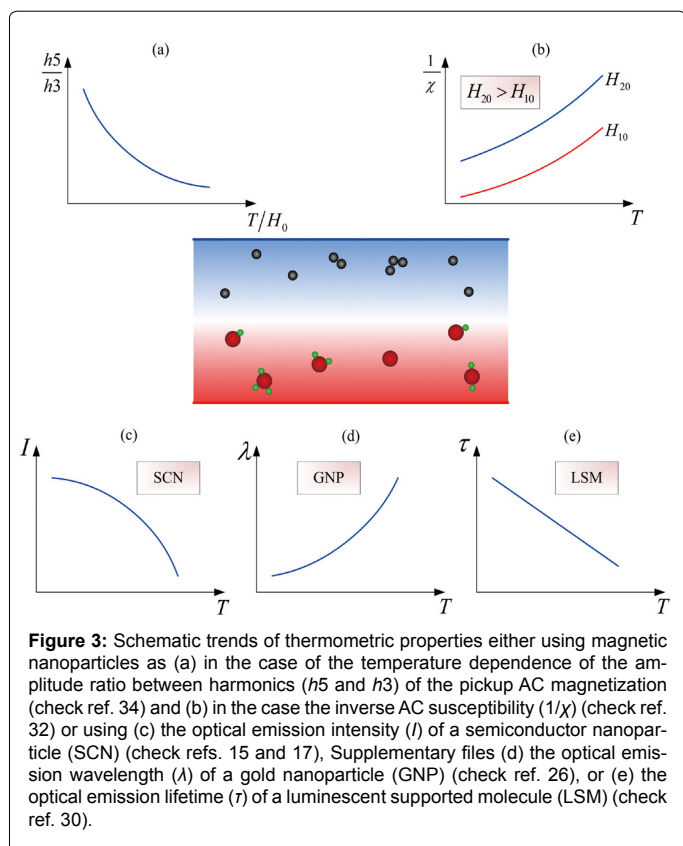
$$M = \phi M_s [\coth(\xi) - (1/\xi)], \quad (7)$$

where ϕ is the particle volume fraction within the sample. The argument $\xi = M_s V H / kT$ in the Langevin function involves the particle's volume (V) and the saturation magnetization (M_s). Equation (7) reveals a monotonic increase of M as ξ increases, i.e. as the T decreases for a fixing value of H . This biunivocal relationship between M and T allows (in principle) one to use the magnetization as the thermometric property. Alternatively, the low-field magnetic susceptibility ($\chi = H/M$) derived from Eq (7) can be used as the thermometric property. Actually, at low values of applied field ($\xi = M_s V H / kT \ll 1$) the Langevin function can be expanded in a Taylor series, leading to an approximate linear relationship between the inverse susceptibility ($1/\chi$) and the temperature (T):

$$1/\chi = H_0 / M \approx 3kT / \phi M_s^2. \quad (8)$$

The choice for using either M or χ as the thermometric property depends on a couple of key factors. The first one is related to the instrumentation required for assessing the parameter (M or χ) with the expected accuracy, sensitivity, robustness, and cost. The second aspect is the algorithm employed to extract T from the measured M or χ data sheet at a given computer cost and noise level.

One approach to extract T from the measured magnetization (M) data sheet is using alternate magnetic fields (AC field approach). Then, the external applied H field can be written as $H = H_0 \cos(\omega t)$, where H_0 is the applied field amplitude and ω is the applied field frequency. While applying the AC field the sample's magnetization responds periodically



and may be expanded in a Fourier series. The contributions of the Fourier components can be checked against the coefficient $\xi_0 = M_s V H_0 / kT$. It is found that the amplitudes of both third and fifth harmonics increase monotonically with ξ_0 , thus providing a biunivocal relationship with T . Actually, the amplitudes of both third and fifth harmonics are also linearly correlated with ϕ . Therefore, the ratio between the fifth and the third harmonic amplitudes is independent of the particle volume fraction within the sampling volume and thus provides a suitable thermometric property. This approach for temperature measurement has been successfully used by Weaver and co-workers and provides accuracy as good as 0.3°C for measurements in the range of 20 to 50°C [33-35].

The alternative approach to extract T uses the inverse magnetic susceptibility ($1/\chi$) instead. According to Eq (8) the $1/\chi$ data sheet recorded at low applied fields scales linearly with T , making the $1/\chi$ data a suitable thermometric property. Worth mentioning, however, that the $1/\chi$ approximation described by Eq (8) also scales with the particle volume fraction (ϕ) within the sampling volume and needs to be considered accordingly. As pointed out before the algorithm employed to extract T from the measured χ data sheet is a key aspect. A successful approach for temperature measurement using magnetic susceptibility data recorded at low applied fields was put forward by Zhong et al. [32]. In this case the authors used Eq (7) to write down the inverse susceptibility while performing a Taylor series expansion up to higher order:

$$1/\chi \approx 3kT/\phi M_s^2 + H_0^2/5\phi kT - M^2 H_0^4/175\phi k^3 T^3 + \dots \quad (9)$$

Then, a data sheet comprising n -pairs ($1/\chi_n \times H_n$) of points can be experimentally obtained for a sampling volume at temperature T containing nanosized magnetic particles at a given particle volume fraction (ϕ). From the higher-order expansion described in Eq (9) a nonlinear matrix formulation can be cast in order to extract T from the experimental values of χ . Using this protocol for temperature measurement Zhong and co-workers reported temperature accuracy better than 0.6°C in the range of 10 to 50°C [32].

Both approaches described in this section, namely optical- and magnetic-based nanothermometry, offer a very positive scenario for breakthroughs in accuracy (meaning the degree of closeness of the measured thermometric property to the reference temperature value) as well as in sensitivity (meaning the amount of change in the thermometric property per unit change in temperature) as long as improvements on signal detection and data manipulation can be realized. Figure 3 collects the trends of the magnetic- and optical-based nanothermometric properties. The central picture of Figure 3 highlights magnetic nanoparticles in the upper part (dark grey spheres) and semiconductor/metal nanoparticles in the lower part (red spheres) supporting or not luminescent moieties (green spots). The two magnetic-based nanothermometric properties are related to remote excitation using AC magnetic fields. While Figure 3a shows the trend of the ratio between harmonics (h_5/h_3) of the sample's magnetization response versus temperature over amplitude of the AC field (T/H_0) [34] Figure 3b presents the typical trend of the inverse AC susceptibility ($1/\chi$) versus temperature (T) at increasing amplitudes of the AC field (H_0) [32]. The three optical-based nanothermometric properties emphasized include the trends reported for the temperature (T) dependence of the optical emission intensity (I) in Figure 3c for a typical semiconductor nanoparticle (SNP) [15,17], the shift in the emission wavelength (λ) for a typical GNP [26] in Figure 3d and the lifetime (τ) variation for a typical luminescent supported moiety (LSM) [30].

Remote nanoparticle-based nanothermometry is far from being exhausted by employing spherically-shaped semiconductor/metal and magnetic nanoparticles. Non-spherically-shaped metallic nanoparticles, such as silver [51] and gold [66], present suitable thermometric properties strongly dependent upon the size and shape [24,62,142]. Actually, nanothermometry can be realized using different nanosized materials, as for instance the heavily-doped (Nd^{3+}) rare-earth-based (LaF_3) nanoparticle, which has been successfully tested not only for nanothermometry but also for magnetohyperthermia [143]. Likewise, carbon-based nanosized structures can also be used as a material platform to build nanothermometers [144]. Worth mentioning the use of nitrogen-vacancy centers in nanodiamonds as nanothermometers [145], including its use to assess the temperature of living cells [146].

Conclusion

Remote hyperthermia (HT), using site-delivered nanosized materials, particularly magnetic-based nanoparticles, is a successful technological approach. The use of remote magnetohyperthermia (MHT) as a therapeutic oncological modality has already reached the clinical trial status with very promising outcomes in patients with recurrence cancer after conventional treatments, such as radiotherapy and chemotherapy. Production of biocompatible nanosized magnetic materials to support the MHT as a therapeutic modality has reached already its maturity, including surface functionalization with smart moieties, aiming to target specific cells and tissues. Legging behind the use of nanosized magnetic particles for remote HT in clinic are nanosized metallic particles remotely excited via radio frequency fields or near infrared light. Likewise, the use of remote HT for controlled release of therapeutic molecules has not reached the clinic, despite the reported breakthroughs while tested in *in vivo* assays. Nevertheless, the lack of a remote technological approach to monitor the targeted site temperature is the gap that needs to be bridged in order to market the clinic remote HT technology on a large scale, no matter how mature remote HT by itself may develop in the coming years. Remote nanothermometry has a huge potential to bridge this gap, providing biocompatible, robust, accurate and cost effective solutions in the short term. Regarding the nanothermometric properties available nowadays, mainly focused on magnetic or optical properties of nanosized materials, the available data point out towards the former as the most promising one. Exciting magnetically and recording magnetic signals from magnetic nanosized materials while targeting deep tissues and internal organs are much more feasible, given the limitation imposed by the optical therapeutic window which narrows both the wavelength range of operation and tissue penetration. We hope this review can contribute to drive the experimental and theoretical work currently underway in the field of remote nanothermometry to better support the establishment of reliable protocols in order to assist the global marketing of the hyperthermia technology for clinical applications.

References

1. Rosensweig RE (2002) Heating magnetic fluid with alternating magnetic field. J Magn Magn Mater 252: 370-374.
2. Vallejo-Fernandez G, Whear O, Roca AG, Hussain S, Timmis, et al. (2013) Mechanisms of hyperthermia in magnetic nanoparticles. J Phys D: Appl Phys 46: 312001.
3. Dombrowsky LA, Timchenko V, Jackson M, Yeoh GH (2011) A combined transient thermal model for laser hyperthermia of tumors with embedded gold nanoshells. Int J Heat Mass Transfer 54: 5459-5469.
4. Patra CR, Cao S, Safgren S, Hattacharya R, Ames MM, et al. (2008) Intracellular Fate of a Targeted Delivery System. J Biomedical Nanotechnol 4: 508-514.

5. Curley SA (2008) Radiofrequency ablation versus resection for resectable colorectal liver metastases: Time for a randomized trial? *Annals Surg Oncol* 15: 11-13.
6. Mambula SS, Calderwood SK (2006) Heat induced release of Hsp70 from prostate carcinoma cells involves both active secretion and passive release from necrotic cells. *Int J Hyperthermia* 22: 575-585.
7. Fagnoni FF, Zerbini A, Pelosi G, Missale G (2008) Combination of radiofrequency ablation and immunotherapy. *Front Biosci* 13: 369-381.
8. Hocine S, Li M-H (2013) Thermoresponsive self-assembled polymer colloids in water. *Soft Matter* 9: 5839-5861.
9. Ward MA, Georgiou TK (2011) Thermoresponsive polymers for biomedical applications. *Polymers* 3: 1215-1242.
10. Sanson C, Diou O, Thévenot J, Ibarboure E, Soum A, et al. (2011) Doxorubicin loaded magnetic polymersomes: theranostic nanocarriers for MR imaging and magneto-chemotherapy. *ACS Nano* 5: 1122-1140.
11. Jiang S, Eltoukhy AA, Love KT, Langer R, Anderson DG (2013) Lipidoid-coated iron oxide nanoparticles for efficient DNA and siRNA delivery. *Nano Lett* 13: 1059-1064.
12. Stanley SA, Gagner JE, Damanpour S, Yoshida M, Dordick JS, et al. (2012) Radio-wave heating of iron oxide nanoparticles can regulate plasma glucose in mice. *Science* 336: 604-608.
13. Johannsen M, Gneveckow U, Thiesen B, Taymoorian K, Cho CH (2007) Thermotherapy of prostate cancer using magnetic nanoparticles: Feasibility, imaging, and three-dimensional temperature distribution. *Eur Urol* 52: 1653-1662.
14. Salloum M, Ma R, Zhu L (2008) An *in-vivo* experimental study of temperature elevations in animal tissue during magnetic nanoparticle hyperthermia. *Int J Hyperthermia* 24: 589-601.
15. Wang S, Westcott S, Chen W (2002) Nanoparticle luminescence thermometry. *J Phys Chem B* 106: 11203-11209.
16. Lee J, Govorov AO, Kotov NA (2005) Nanoparticle assemblies with molecular springs: a nanoscale thermometer. *Angew Chem Int Ed Engl* 44: 7439-7442.
17. Wu T, Zou G, Hu J, Liu S (2009) Fabrication of photoswitchable multicolor fluorescent hybrid silica nanoparticles coated with dye-labeled poly(N-isopropylacrylamide) brushes. *Chem Mater* 21: 3788-3798.
18. Wu W, Shen J, Banerjee P, Zhou S (2010) Core-shell hybrid nanogels for integration of optical temperature-sensing, targeted tumor cell imaging, and combined chemo-photothermal treatment. *Biomaterials* 31: 7555-7566.
19. Ye F, Wu C, Jin Y, Chan YH, Zhang X, et al. (2011) Radiometric temperature sensing with semiconducting polymer dots. *J Am Chem Soc* 133: 8146-8149.
20. Peng H-S, Huang S-H, Wolfbeis OS (2010) Radiometric fluorescence nanoparticles for sensing temperature. *J Nanopart Res* 12: 2729-2733.
21. Fischer LH, Harms GS, Wolfbeis OS (2011) Upconverting nanoparticles for nanoscale thermometry. *Angew Chem Int Ed Engl* 50: 4546-4551.
22. Brites CD, Lima PP, Silva NJ, Millán A, Amaral VS, et al. (2012) Thermometry at the nanoscale. *Nanoscale* 4: 4799-4829.
23. Riedinger A, Guardia P, Curcio A, Garcia MA, Cingolani R, et al. (2013) Subnanometer local temperature probing and remotely controlled drug release based on azo-functionalized iron oxide nanoparticles. *Nano Lett* 13: 2399-2406.
24. Flourous NJ, Saitoh K, Koshiba M (2007) Numerical modelling of cryogenic temperature sensors based on plasmonic oscillations in metallic nanoparticles embedded into photonic crystal fibers. *IEEE Photon Technol Lett* 19: 324-326.
25. Gupta A, Kane RS, Borca-Tasciuc D-A (2010) Local temperature measurements in the vicinity of electromagnetically heated magnetite and gold nanoparticles. *J App Phys* 108: 064901.
26. Setoura K, Werner D, Hashimoto S (2012) Optical scattering spectral thermometry and refractometry of a single gold nanoparticle under CW laser excitation. *J Phys Chem C* 116: 15458-15466.
27. Sun L-N, Yu J, Peng H, Zhang JZ, Shi L-Y (2010) Temperature-sensitive luminescent nanoparticles and films based on a Terbium (III) complex probe. *J Phys Chem C* 114: 12642-12648.
28. Chen S, Hoskins C, Wang L, MacDonald MP, André P (2012) A water-soluble temperature nanoprobe based on a multimodal magnetic-luminescent nanocolloid. *Chem Commun (Camb)* 48: 2501-2503.
29. Jaque D, Vetrone F (2012) Luminescence nanothermometry. *Nanoscale* 4: 4301-4326.
30. Freddi S, Sironi L, D'Antuono R, Morone D, Donà A, et al. (2013) A molecular thermometer for nanoparticles for optical hyperthermia. *Nano Lett* 13: 2004-2010.
31. Passos SK, de Souza PEN, Soares PKP, Eid DRM, Primo FL, et al. (2013) A quantitative approach for skin field cancerization using a nanoencapsulated PDT-agent: A pilot study. *Clinic Cosmet Invest Dermat* 6: 51-59.
32. Zhong J, Liu W, Du Z, César de Morais P, Xiang Q, et al. (2012) A noninvasive, remote and precise method for temperature and concentration estimation using magnetic nanoparticles. *Nanotechnology* 23: 075703.
33. Rauwerdink AM, Hansen EW, Weaver JB (2009) Nanoparticle temperature estimation in combined ac and dc magnetic fields. *Phys Med Biol* 54: L51-55.
34. Weaver JB, Rauwerdink AM, Hansen EW (2009) Magnetic nanoparticle temperature estimation. *Med Phys* 36: 1822-1829.
35. Weaver JB (2012) The use of magnetic nanoparticles in thermal therapy monitoring and screening: Localization and imaging (invited). *J Appl Phys* 111: 7B317-317B3173.
36. Wust P, Gneveckow U, Johannsen M, Böhmer D, Henkel T, et al. (2006) Magnetic nanoparticles for interstitial thermotherapy—feasibility, tolerance and achieved temperatures. *Int J Hyperthermia* 22: 673-685.
37. Jaque D, Martínez Maestro L, del Rosal B, Haro-Gonzalez P, Benayas A, Plaza JL, Martín Rodríguez E, García Solé J (2014) Nanoparticles for photothermal therapies. *Nanoscale* (accepted paper DOI: 10.1039/C4NR00708E).
38. Curley SA (2001) Radiofrequency ablation of malignant liver tumors. *Oncologist* 6: 14-23.
39. Cavagnaro M, Amabile C, Bernardi P, Pisa S, Tosoratti N (2011) A minimally invasive antenna for microwave ablation therapies: design, performances, and experimental assessment. *IEEE Trans Biomed Eng* 58: 949-959.
40. Gannon CJ, Patra CR, Bhattacharya R, Mukherjee P, Curley SA (2008) Intracellular gold nanoparticles enhance non-invasive radiofrequency thermal destruction of human gastrointestinal cancer cells. *J Nanobiotechnology* 6: 2.
41. Wust P, Hildebrandt B, Sreenivasa G, Rau B, Gellermann J, et al. (2002) Hyperthermia in combined treatment of cancer. *Lancet Oncol* 3: 487-497.
42. Hildebrandt B, Wust P, Ahlers O, Dieing A, Sreenivasa G, et al. (2002) The cellular and molecular basis of hyperthermia. *Crit Rev Oncol Hematol* 43: 33-56.
43. Milleron RS, Bratton SB (2007) 'Heated' debates in apoptosis. *Cell Mol Life Sci* 64: 2329-2333.
44. Cherukuri P, Glazer ES, Curley SA (2010) Targeted hyperthermia using metal nanoparticles. *Adv Drug Deliv Rev* 62: 339-345.
45. Kennedy LC, Bickford LR, Lewinski NA, Coughlin AJ, Hu Y, et al. (2011) A new era for cancer treatment: gold-nanoparticle-mediated thermal therapies. *Small* 7: 169-183.
46. Qin Z, Bischof JC (2012) Thermophysical and biological responses of gold nanoparticle laser heating. *Chem Soc Rev* 41: 1191-1217.
47. Honda M, Saito Y, Smith NI, Fujita K, Kawata S (2011) Nanoscale heating of laser irradiated single gold nanoparticles in liquid. *Opt Express* 19: 12375-12383.
48. Contreras-Cáceres R, Pacifico J, Pastoriza-Santos I, Pérez-Juste J, Fernández-Barbero A, Liz-Marzán LM (2009) Au@pNIPAM Thermosensitive Nanostructures: Control over Shell Cross-linking, Overall Dimensions, and Core Growth. *Adv Funct Mater* 19: 3070-3076.
49. Brust M, Walker M, Bethell D, Schiffrin DJ, Whyman R (1994) Synthesis of thiol-derivatised gold nanoparticles in two-phase liquid-liquid system. *J Chem Soc Chem Commun* 801-802.
50. Gibson JD, Khanal BP, Zubarev ER (2007) Paclitaxel-functionalized gold nanoparticles. *J Am Chem Soc* 129: 11653-11661.
51. Langille MR, Personick ML, Mirkin CA (2013) Plasmon-mediated syntheses of metallic nanostructures. *Angew Chem Int Ed Engl* 52: 13910-13940.
52. Everts M, Saini V, Leddon JL, Kok RJ, Stoff-Khalili M, et al. (2006) Covalently linked Au nanoparticles to a viral vector: potential for combined photothermal and gene cancer therapy. *Nano Lett* 6: 587-591.

53. Su Y, Wei X, Peng F, Zhong Y, Lu Y, et al. (2012) Gold nanoparticles-decorated silicon nanowires as highly efficient near-infrared hyperthermia agents for cancer cells destruction. *Nano Lett* 12: 1845-1850.
54. Vigderman L, Zubarev ER (2013) Therapeutic platforms based on gold nanoparticles and their covalent conjugates with drug molecules. *Adv Drug Deliv Rev* 65: 663-676.
55. Dreaden EC, Mwakwari SC, Sodji QH, Oyelere AK, El-Sayed MA (2009) Tamoxifen-poly(ethylene glycol)-thiol gold nanoparticle conjugates: enhanced potency and selective delivery for breast cancer treatment. *Bioconjug Chem* 20: 2247-2253.
56. Lee H, Kang T, Yoon KA, Lee SY, Joo SW, et al. (2010) Colorimetric detection of mutations in epidermal growth factor receptor using gold nanoparticle aggregation. *Biosens Bioelectron* 25: 1669-1674.
57. Barua S, Mitragotri S (2013) Synergistic targeting of cell membrane, cytoplasm, and nucleus of cancer cells using rod-shaped nanoparticles. *ACS Nano* 7: 9558-9570.
58. Berry CC (2008) Intracellular delivery of nanoparticles via the HIV-1 tat peptide. *Nanomedicine (Lond)* 3: 357-365.
59. Eustis S, el-Sayed MA (2006) Why gold nanoparticles are more precious than pretty gold: noble metal surface plasmon resonance and its enhancement of the radiative and nonradiative properties of nanocrystals of different shapes. *Chem Soc Rev* 35: 209-217.
60. Weissleder R (2001) A clearer vision for in vivo imaging. *Nat Biotechnol* 19: 316-317.
61. Kamat PV (2002) Photophysical, photochemical and photocatalytic aspects of metal nanoparticles. *J Phys Chem B* 106: 7729-7744.
62. Jain PK, Lee KS, El-Sayed IH, El-Sayed MA (2006) Calculated absorption and scattering properties of gold nanoparticles of different size, shape, and composition: applications in biological imaging and biomedicine. *J Phys Chem B* 110: 7238-7248.
63. Day ES, Morton JG, West JL (2009) Nanoparticles for thermal cancer therapy. *J Biomech Eng* 131: 074001.
64. Gobin AM, Lee MH, Halas NJ, James WD, Drezek RA, et al. (2007) Near-infrared resonant nanoshells for combined optical imaging and photothermal cancer therapy. *Nano Lett* 7: 1929-1934.
65. Martos-Maldonado MC, Thygesen MB, Jensen KJ, Vargas-Berenguel A (2013) Gold-Ferrocene Glyco-Nanoparticles for High-Sensitivity Electrochemical Detection of Carbohydrate-Lectin Interactions. *Eur J Org Chem* 2793-2801.
66. Myroshnychenko V, Rodríguez-Fernández J, Pastoriza-Santos I, Funston AM, Novo C, et al. (2008) Modelling the optical response of gold nanoparticles. *Chem Soc Rev* 37: 1792-1805.
67. Modest M (2003) Radiative Heat Transfer. Academic Press, Burlington, Massachusetts, USA.
68. Elliott AM, Stafford RJ, Schwartz J, Wang J, Shetty AM, et al. (2007) Laser-induced thermal response and characterization of nanoparticles for cancer treatment using magnetic resonance thermal imaging. *Med Phys* 34: 3102-3108.
69. Elliott AM, Schwartz J, Wang J, Shetty AM, Bourgoyne C, et al. (2009) Quantitative comparison of delta P1 versus optical diffusion approximations for modeling near-infrared gold nanoshell heating. *Med Phys* 36: 1351-1358.
70. Massart R (1981) Preparation of aqueous magnetic liquids in alkaline and acid media. *IEEE Trans Magn* 17: 1247-1248.
71. Morais PC, Garg VK, Oliveira AC, Silva LP, Azevedo RB, et al. (2001) Synthesis and characterization of size-controlled cobalt ferrite-based ionic ferrofluids. *J Magn Magn Mater* 225: 37-40.
72. Si S, Kotal A, Mandal TK, Giri S, Nakamura H, et al. (2004) Size-controlled synthesis of magnetite nanoparticles in the presence of polyelectrolytes. *Chem Mater* 16: 3489-3496.
73. Lee DC, Smith DK, Heitsch AT, Korgel BA (2007) Colloidal magnetic nanocrystals: synthesis, properties and applications. *Annual Rep Section C Phys Chem* 103: 351-402.
74. Hyeon T, Lee SS, Park J, Chung Y, Na HB (2001) Synthesis of highly crystalline and monodisperse maghemite nanocrystallites without a size-selection process. *J Am Chem Soc* 123: 12798-12801.
75. Sun S, Zeng H (2002) Size-controlled synthesis of magnetite nanoparticles. *J Am Chem Soc* 124: 8204-8205.
76. Roca AG, Costo R, Rebolledo AF, Veintemillas-Verdaguer S, Tartaj P, et al. (2009) Progress in the preparation of magnetic nanoparticles for applications in biomedicine. *J Phys D: Appl Phys* 42: 224002.
77. Morais PC, Santos RL, Pimenta ACM, Azevedo RB, Lima ECD (2006) Preparation and characterization of ultra-stable biocompatible magnetic fluids using citrate-coated cobalt ferrite nanoparticles. *Thin Sol Films* 515: 266-270.
78. Soler MA, Lima EC, Nunes ES, Silva FL, Oliveira AC, et al. (2011) Spectroscopic study of maghemite nanoparticles surface-grafted with DMSA. *J Phys Chem A* 115: 1003-1008.
79. Monge-Fuentes V, Garcia MP, Tavares MC, Valois CR, Lima EC, et al. (2011) Biodistribution and biocompatibility of DMSA-stabilized maghemite magnetic nanoparticles in nonhuman primates (*Cebus spp.*). *Nanomedicine (Lond)* 6: 1529-1544.
80. Ruiz A, Salas G, Calero M, Hernández Y, Villanueva A, et al. (2013) Short-chain PEG molecules strongly bound to magnetic nanoparticle for MRI long circulating agents. *Acta Biomater* 9: 6421-6430.
81. Santos CMB, da Silva SW, Guilherme LR, Morais PC (2011) SERRS study of molecular arrangement of Amphotericin B adsorbed onto iron oxide nanoparticles precoated with a bilayer of lauric acid. *J Phys Chem C* 115: 20442-20448.
82. Santos CMB, da Silva SW, Saldanha CA, Almeida Santos MFM, Garcia MP, et al. (2013) SERS as a valuable tool for detection and diagnostic and treatment follow-up of fungal infection in mice lungs: Use of Amphotericin B and its nanoencapsulation onto magnetic nanoparticles. *J Raman Spectrosc* 44: 695-702.
83. Zhang S, Bian Z, Gu C, Zhang Y, He S, et al. (2007) Preparation of anti-human cardiac troponin I immunomagnetic nanoparticles and biological activity assays. *Colloids Surf B Biointerfaces* 55: 143-148.
84. da Paz MC, Santos Mde F, Santos CM, da Silva SW, de Souza LB, et al. (2012) Anti-CEA loaded maghemite nanoparticles as a theragnostic device for colorectal cancer. *Int J Nanomedicine* 7: 5271-5282.
85. Sharma R, Chen CJ (2009) Newer nanoparticles in hyperthermia treatment and thermometry. *J Nanoparticle Res* 11: 671-689.
86. Hilger I, Kaiser WA (2012) Iron oxide-based nanostructures for MRI and magnetic hyperthermia. *Nanomedicine (Lond)* 7: 1443-1459.
87. Branquinho LC, Carrião MS, Costa AS, Zufelato N, Sousa MH, et al. (2013) Effect of magnetic dipolar interactions on nanoparticle heating efficiency: implications for cancer hyperthermia. *Sci Rep* 3: 2887.
88. Morais PC, Santos JG, Silveira LB, Gansau C, Buske N, et al. (2004) Susceptibility investigation of the nanoparticle coating-layer effect on the particle interaction in biocompatible magnetic fluids. *J Magn Magn Mater* 272-276: 2328-2329.
89. Soler MAG, Paterno LG, Sinnecker JP, Wen JG, Sinnecker EHCP, et al. (2012) Assembly of γ -Fe₂O₃/polyaniline nanofilms with tuned dipolar interaction. *J Nanopart Res* 14: 653.
90. Rabelo D, Lima ECD, Reis AC, Nunes WC, Novak MA, et al. (2001) Preparation of magnetite nanoparticles in mesoporous copolymer template. *Nano Lett* 1: 105-108.
91. Ohno K, Koh K, Tsujii Y, Fukuda T (2002) Synthesis of gold nanoparticles coated with well-defined, high-density polymer brushes by surface-initiated living radical polymerization *Macromolecules* 35: 8989-8993.
92. Morais PC, Azevedo RB, Rabelo D, Lima ECD (2003) Synthesis of magnetite nanoparticles in mesoporous copolymer template: A model system for mass-loading control. *Chem Mater* 15: 2485-2487.
93. Rodriguez AF, Coaquira JA, Morales MA, Faria FS, Cunha RM, et al. (2013) Synthesis, characterization and magnetic properties of polymer-Fe₃O₄ nanocomposite. *Spectrochim Acta A Mol Biomol Spectrosc* 100: 101-103.
94. Pedroza RC, da Silva SW, Soler MAG, Sartoratto PPC, Resende DR, et al. (2005) Raman study of nanoparticle-template interaction in a CoFe₂O₄/SiO₂-based nanocomposite prepared by sol-gel method. *J Magn Magn Mater* 289: 139-141.
95. Simioni AR, Primo FL, Rodrigues MA, Lacava ZGM, Morais PC, et al. (2007) Preparation, characterization and in vitro toxicity test of magnetic nanoparticle-based drug delivery system to Hyperthermia of biological tissues. *IEEE Trans Magn* 43: 2459-2461.

96. Paterno LG, Fonseca FJ, Soler MAG, Bao SN, Morais PC, et al. (2009) Fabrication and characterization of nanostructured conducting polymer films containing magnetic nanoparticles. *Thin Sol Films* 517: 1753-1758.
97. Paterno LG, Soler MAG, Fonseca FJ, Sinnecker JP, Sinnecker EHCP, et al. (2009) Layer-by-layer assembly of bi-functional nanofilms: Surface-functionalized maghemite hosted in polyaniline. *J Phys Chem C* 113: 5087-5095.
98. Alcantara GB, Paterno LG, Afonso AS, Faria RC, Pereira-da-Silva MA, et al. (2011) Adsorption of cobalt ferrite nanoparticles within layer-by-layer films: a kinetic study carried out using quartz crystal microbalance. *Phys Chem Chem Phys* 13: 21233-21242.
99. Oliveira DM, Macaroff PP, Ribeiro KF, Lacava ZGM, Azevedo RB, et al. (2005) Studies of zinc phthalocyanine/magnetic fluid complex as a bifunctional agent for cancer treatment. *J Magn Magn Mater* 289: 476-479.
100. Morais PC, Silveira LB, Oliveira AC, Lacava BM, Tedesco AC, et al. (2008) Dynamic susceptibility investigation of maghemite nanoparticles incorporated in bovine serum albumin template. *J Nanosci Nanotechnol* 8: 2684-2687.
101. Amaral AC, Bocca AL, Ribeiro AM, Nunes J, Peixoto DL, et al. (2009) Amphotericin B in poly(lactic-co-glycolic acid) (PLGA) and dimercaptosuccinic acid (DMSA) nanoparticles against paracoccidiodomycosis. *J Antimicrob Chemother* 63: 526-533.
102. Rodrigues MMA, Simioni AR, Primo FL, Siqueira-Moura MP, Morais PC, et al. (2009) Preparation, characterization and in vitro cytotoxicity of the BSA nanoparticles containing magnetic fluid and/or photosensitizer. *J Magn Magn Mater* 321: 1600-1603.
103. Simioni AR, Rodrigues MM, Primo FL, Morais PC, Tedesco AC (2011) Effect of diode-laser and AC magnetic field of bovine serum albumin nanospheres loaded with phthalocyanine and magnetic particles. *J Nanosci Nanotechnol* 11: 3604-3608.
104. Estevanato L, Cintra D, Baldini N, Portilho F, Barbosa L, et al. (2011) Preliminary biocompatibility investigation of magnetic albumin nanosphere designed as a potential versatile drug delivery system. *Int J Nanomedicine* 6: 1709-1717.
105. Cintra e Silva Dde O, Estevanato LL, Simioni AR, Rodrigues MM, Lacava BM, et al. (2012) Successful strategy for targeting the central nervous system using magnetic albumin nanospheres. *J Biomed Nanotechnol* 8: 182-189.
106. Bolfarin GC, Siqueira-Moura MP, Demets GJF, Morais PC, Tedesco AC (2012) In vitro evaluation of combined hyperthermia and photodynamic effects using magnetoliposomes loaded with cucurbit[7]uril zinc phthalocyanine complex on melanoma. *J Photochem B Biol* 115: 1-4.
107. Vaccari CB, Cerize NN, Morais PC, Ré MI, Tedesco AC (2012) Biocompatible magnetic microspheres for Use in PDT and hyperthermia. *J Nanosci Nanotechnol* 12: 5111-5116.
108. Estevanato LL, Da Silva JR, Falqueiro AM, Mosiniewicz-Szablewska E, Suchocki P, et al. (2012) Co-nanoencapsulation of magnetic nanoparticles and selol for breast tumor treatment: in vitro evaluation of cytotoxicity and magnetohyperthermia efficacy. *Int J Nanomedicine* 7: 5287-5299.
109. Macaroff PP, Oliveira DM, Lacava ZGM, Lima ECD, Morais PC, et al. (2005) Investigation of pheophorbide/magnetic fluid complex as a promising system for early cancer detection and treatment. *J Appl Phys* 97: 10Q906.
110. Oliveira DM, Lacava ZG, Lima EC, Morais PC, Tedesco AC (2006) Zinc phthalocyanine/magnetic fluid complex: a promising dual nanostructured system for cancer treatment. *J Nanosci Nanotechnol* 6: 2432-2437.
111. Primo FL, Michieletto L, Rodrigues MMA, Macaroff PP, Morais PC, et al. (2007) Magnetic nanoemulsions as drug delivery system for Foscan: Permeation and retention in vitro assays for topical application in photodynamic therapy (PDT) of skin-cancer. *J Magn Magn Mater* 311: 354-357.
112. de Paula LB, Primo FL, Jardim DR, Morais PC, Tedesco AC (2012) Development, characterization and in vitro trials of chloroaluminum phthalocyanine-magnetic nanoemulsion to hyperthermia and photodynamic therapies on glioblastoma as biological model. *J Appl Phys* 111: 07B307.
113. Carneiro ML, Peixoto RC, Joanitti GA, Oliveira RG, Telles LA, et al. (2013) Antitumor effect and toxicity of free rhodium (II) citrate and rhodium (II) citrate-loaded maghemite nanoparticles in mice bearing breast cancer. *J Nanobiotechnology* 11: 4.
114. Nunes ES, Carneiro MLB, Oliveira RGS, Bao SN, Souza AR (2013) Colloidal stability, surface characterisation and intracellular accumulation of Rhodium(II) citrate coated superparamagnetic iron oxide nanoparticles in breast tumour: a promising platform for cancer therapy. *J Nanopart Res* 15: 1683.
115. Aslan K, Perez-Luna VH (2006) Nonradiative interactions between biotin-functionalized gold nanoparticles and fluorophore-labeled anti-biotin. *Plasmonics* 1: 111-119.
116. Yoon H-J, Jang W-D (2010) Polymeric supramolecular systems for drug delivery. *J Mater Chem* 20: 211-222.
117. Alexander A, Ajazuddin, Khan J, Saraf S, Saraf S (2013) Poly(ethylene glycol)-poly(lactic-co-glycolic acid) based thermosensitive injectable hydrogels for biomedical applications. *J Control Release* 172: 715-729.
118. Schattling P, Jochum FD, Theato P (2014) Multi-stimuli responsive polymers – the all-in-one talents. *Polym Chem* 5: 25-36.
119. Lutz JF (2008) Polymerization of oligo(ethylene glycol)(meth)acrylates: Toward new generations of smart biocompatible materials. *J Polym Sci Part A* 46: 3459-3470.
120. Trivedi R, Kompella UB (2010) Nanocellular formulations for sustained drug delivery: strategies and underlying principles. *Nanomedicine (Lond)* 5: 485-505.
121. Tsitsilianis C (2010) Responsive reversible hydrogels from associative “smart” macromolecules. *Soft Matter* 6: 2372-2388.
122. Blanazs A, Armes SP, Ryan AJ (2009) Self-Assembled Block Copolymer Aggregates: From Micelles to Vesicles and their Biological Applications. *Macromol Rapid Commun* 30: 267-277.
123. Meng F, Zhong Z, Feijen J (2009) Stimuli-responsive polymersomes for programmed drug delivery. *Biomacromolecules* 10: 197-209.
124. Meenach SA, Anderson KW, Hilt JZ (2010) Synthesis and characterization of thermoresponsive poly(ethylene glycol)-based hydrogels and their magnetic nanocomposites. *J Polym Sci Part A* 48: 3229-3235.
125. Papaphilipou PC, Pourgouris A, Marinica O, Taculescu A, Athanasopoulos GI, et al. (2011) Fabrication and characterization of superparamagnetic and thermoresponsive hydrogels based on oleic-acid-coated Fe₃O₄ nanoparticles, hexa(ethylene glycol) methyl ether methacrylate and 2-(acetoacetoxy)ethyl methacrylate. *J Magn Magn Mater* 323: 557-563.
126. Liu T-Y, Hu S-H, Liu D-M, Chen SY, Chen IW (2009) Biomedical nanoparticle carriers with combined thermal and magnetic responses. *Nano Today* 4: 52-65.
127. Zhao X-Q, Wang T-X, Liu W, Wang CD, Wang D, et al. (2011) Multifunctional Au@IPN-pNIPAAm nanogels for cancer cell imaging and combined chemophotothermal treatment. *J Mater Chem* 21: 7240-7247.
128. Wilson OM, Hu X, Cahill DG, Braun PV (2002) Colloidal metal particles as probes of nanoscale thermal transport in fluids. *Phys Rev B* 66: 224301.
129. Swartz ET, Pohl RO (1989) Thermal boundary resistance. *Rev Mod Phys* 61: 605-668.
130. Baffou G, Quidant R, Girard C (2010) Thermoplasmonics modeling: A Green's function approach. *Phys Rev B* 82: 165424.
131. Alper J, Hamad-Schifferli K (2010) Effect of ligands on thermal dissipation from gold nanorods. *Langmuir* 26: 3786-3789.
132. Kordas J, Avouris P, El-Bayoumi A (1975) Effect of temperature on the oscillator strength of a nonrigid molecule. *J Phys Chem* 79: 2420-2423.
133. Bohren CF, Huffman DR (1983) Absorption and scattering of light by small particles. Wiley, Mörlenbach, Germany.
134. Jahan NA, Hermannstadter C, Huh J-H, Sasakura H, Rotter TJ, et al. (2013) Temperature dependent carrier dynamics in telecommunication band InAs quantum dots and dashes grown on InP substrates. *J Appl Phys* 113: 033506.
135. Vurgafman I, Meyer JR, Ram-Mohan LR (2001) Band parameters for III-V compound semiconductors and their alloys. *J Appl Phys* 89: 5815-5875.
136. O'Donnell KP, Chen X (1991) Temperature dependence of semiconductor band gaps. *Appl Phys Lett* 58: 2924-2926.
137. Olkhovets A, Hsu R-C, Lipovskii A, Wise FW (1998) Size-Dependent Temperature Variation of the Energy Gap in Lead-Salt Quantum Dots. *Phys Rev Lett* 81: 3539-3542.

138. Dai Q, Zhang Y, Wang Y, Hu MZ, Zou B, et al. (2010) Size-dependent temperature effects on PbSe nanocrystals. *Langmuir* 26: 11435-11440.
139. Maestro LM, Jacinto C, Silva UR, Vetrone F, Capobianco JA, et al. (2011) CdTe quantum dots as nanothermometers: towards highly sensitive thermal imaging. *Small* 7: 1774-1778.
140. Maestro LM, Jacinto C, Silva UR, Vetrone F, Capobianco JA, et al. (2013) Response to "Critical growth temperature of aqueous CdTe quantum dots is non-negligible for their application as nanothermometers". *Small* 9: 3198-3200.
141. Felder D, Nierengarten JF, Barigelletti F, Ventura B, Armaroli N (2001) Highly luminescent Cu(I)-phenanthroline complexes in rigid matrix and temperature dependence of the photophysical properties. *J Am Chem Soc* 123: 6291-6299.
142. Grubisic A, Schweikhard V, Baker TA, Nesbitt DJ (2013) Multiphoton photoelectron emission microscopy of single Au nanorods: combined experimental and theoretical study of rod morphology and dielectric environment on localized surface plasmon resonances. *Phys Chem Chem Phys* 15: 10616-10627.
143. Rocha U, Kumar KU, Jacinto C, Ramiro J, Caamaño AJ, et al. (2014) Nd³⁺-doped LaF₃ nanoparticles as self-monitored photo-thermal agents. *Appl Phys Lett* 104: 053703.
144. Osswald S, Behler K, Gogotsi Y (2008) Laser-induced light emission from carbon nanoparticles. *J Appl Phys* 104: 074308.
145. Knowles HS, Kara DM, Atatüre M (2014) Observing bulk diamond spin coherence in high-purity nanodiamonds. *Nat Mater* 13: 21-25.
146. Kucsko G, Maurer PC, Yao NY, Kubo M, Noh HJ, et al. (2013) Nanometre-scale thermometry in a living cell. *Nature* 500: 54-58.